CrossMark

ORIGINAL PAPER

Mechanical behavior of an individual adherent MLO-Y4 osteocyte under shear flow

Jun Qiu[1] · **Fang-Fang Li[2]**

Abstract Mechanical properties of a single cell and its mechanical response under stimulation play an important role in regulating interactions between cell and extracellular matrix and affecting mechanotransduction. Osteocytes exhibit solid-like viscoelastic behavior in response to the interstitial fluid shear resulting from tissue matrix deformation. This study intends to quantitatively describe the mechanical behavior of osteocytes combining in vitro experiment and fluid–structure interaction (FSI) finite element (FE) model. The cell is configured in the FSI FE model using the observed data from quasi-3D images. Instead of simply assigning the cellular viscoelastic parameters by statistical data, the mechanical parameters are determined by an iterative algorithm comparing the experimental and the computational results from the FE model. The viscoelastic parameters of osteocytes are obtained as: the equilibrium elasticity modulus $k_1 = 0.15 \pm 0.038$ kPa, instantaneous elasticity modulus $(k_1 + k_2) = 0.77 \pm 0.23$ kPa, viscosity coefficient $\eta = 1.38 \pm 0.33$ kPa s. A novel index to quantify the cell adhesion is also put forward. In addition, an interesting competition phenomenon is revealed on the cell surface concerning stress and strain, i.e., the place with high stress has low strain and that with low stress has high strain. The proposed method provides a novel technique to study the mechanical behavior of individual adherent cell in vitro. It is believed that this quantitative technique not only determines cell mechanical behavior but also helps elucidate the mechanism of mechanotransduction in various types of cells.

Keywords Viscoelastic · Osteocyte · Shear fluid · Fluid–structure interaction · Finite element modeling · Cell mechanical property

1 Introduction

Osteocytes, mature bone cells embedded in mineralized bone matrix, are under dynamic shear fluid in vivo and exhibit significant viscoelastic behavior (Jacobs et al. 2010). Abundant evidence has shown that osteocytes are the key mechanonsensor cells that directly regulate activities of bone-forming osteoblast and bone-removing osteoclast (You et al. 2008). Thus, osteocytes are critical to etiology and new treatments for osteoporosis. One of the common loading mechanisms on cells such as osteocytes is interstitial fluid shear resulting from tissue matrix deformation (Cowin and Telega 2003; Weinbaum et al. 1994). Such deformation introduces mechanical stress and strain inside cell body, such as stretch and compression, and may trigger the activation and transduction of biochemical signals (Guilak 1995). Although the fluid–structure interactions (FSI) at the cellular level appear to be universal and may hold the key to unraveling the mechanisms of cellular mechanotransduction, they are poorly understood (Anderson et al. 2006).

Knowledge of the structural and mechanical property of the cell is necessary to study the spatial distribution and performing process of the stress/strain in the adherent cell under

✉ Jun Qiu
aeroengine@tsinghua.edu.cn

Fang-Fang Li
liff@cau.edu.cn

1 Institute for Aero-Engine, School of Aerospace Engineering, Tsinghua University, Mailbox H18, Meng Minwei Science and Technology Building, Beijing 100084, People's Republic of China

2 College of Water Resources and Civil Engineering, China Agricultural University, Beijing 100083, People's Republic of China

🌀 Springer

shear flow (Hazel and Pedley 2000). Several traditional *in vitro* techniques have been developed to determine the viscoelastic properties of various cells, including micropipette aspiration (Baaijens et al. 2005; Evans and Yeung 1989; Hochmuth 2000; Sato et al. 1990; Theret et al. 1988), unconfined cell compression (Wu and Herzog 2006), cytoindentation (Koay et al. 2003; Shin and Athanasiou 1999), atomic force microscopy (AFM) (Charras and Horton 2002; Darling et al. 2006; Lulevich et al. 2006; Mahaffy et al. 2004; Vargas-Pinto et al. 2015), magnetic bead rheometry (Bausch et al. 1998), and optical traps (Guck 2005). However, cytoindentation, AFM and magnetic twist methods always apply load locally by probes or beads; thus, the measured mechanical properties only characterize the local nature of the cell. As to micropipette aspiration, unconfined cell compression and optical traps methods, although the entire cell is loaded, there are external objects or energy interposed in the cell during the measurement, which may alter the cell structure and properties.

This study proposes a novel approach combining cell flow experiment and finite element (FE) modeling to noninvasively study the mechanical behavior of a whole cell under fluid flow. The deformation of the osteocytic cell in fluids is recorded by a custom-built dual microscope system named quasi-3D microscopy (Baik et al. 2010), which is able to capture two orthogonal planes of a cell simultaneously at a high temporal resolution. Previous work has validated the accuracy of this observation system (Qiu et al. 2012). An FE model is established to numerically simulate the deformation of an individual cell under shear flow. In the model, the cell configuration is based on the observed data derived from the microscopic images, as opposed to the assumption of a sphere or semi-sphere (Baaijens et al. 2005; Zhao et al. 2009) with statistical dimension or an half-space in the analytical solution (Sato et al. 1990; Theret et al. 1988). Instead of simply assigning the cellular viscoelastic parameters using statistical data from the literatures totally or partially, the parameters of each sample cell are determined individually by an iterative algorithm minimizing the deformation difference between the observed data and the computational results from the FE model, so that the cellular difference induced by biological diversity could be sufficiently considered and reflected.

The contribution of this study is mainly composed of: (1) the establishment of a fluid–structure interactive FE model based on individual cellular data to study the unique mechanical behavior of a particular cell; (2) the determination of the viscoelastic properties of osteocytes using 3D FSI FE model and fluid shear experiments under quasi-3D microscope; (3) the proposal of an index to quantify the cell adhesion on the basis of static friction coefficient; (4) the revelation of an interesting 'competition phenomenon' between stress and strain on the cell surface, i.e., the place with high stress has low strain and that with low stress has high strain.

2 Methodology

2.1 Framework

The main difficulty of modeling an adherent cell lies in the estimation of the cellular viscoelasticity, which can be presented by three parameters in standard linear solid (SLS) viscoelastic model, i.e., k_1, k_2, and η. An iterative method based on the experimental observation and finite element model is thus established to obtain the accurate viscoelastic parameters, the frame work of which is illustrated in Fig. 1.

A custom-built quasi-3D observation system composed of two microscopes (Baik et al. 2010; Qiu et al. 2012) as illustrated in Fig. 2 is used to record the deformation of the cell at different moment from both bottom view and side view. The initial cell contour without shear fluid is firstly adopted to construct a 3D numerical cell for FE model. Hence, unlike most of the studies, in which the numerical cell is usually simplified to a hemispheroid or semi-ellipsoid, the numerical cell here is reconstructed on the basis of the real cellular configurations.

A 3D fluid–structure interaction FE model is then established using the numerical cell under the flow conditions as in experiments. A group of estimated cellular viscoelastic parameters is input to the FE model, and the calculated load-deformation path is compared to the records from the quasi-3D observation system. The group of viscoelastic parameters will be updated if there is a large gap between the simulated deformation process and the experimental observations. The iteration stops until the load-deformation path resulted from the FE model approaches the observations, when the viscoelastic parameters of the cell are determined.

With the viscoelastic parameters of the adherent cell, the force as well as the deformation of the cell under shear fluid can be worked out by the 3D fluid–structure interaction FE model.

2.2 In vitro experiments

2.2.1 Cell culture and cell flow chamber experiments

Osteocytic MLO-Y4 cells (Bonewald and Kato 2002) growing in culture media consisting of α-modified Eagle's medium (α-MEM), 5 % fetal bovine serum, and 5 % calf serum, at 37 °C in a humidified atmosphere of 95 % air and 5 % CO_2 are selected in this study.

Syringe pump (New Era Pump Systems, Wantagh, NY) and gas-tight syringe (Hamilton, Reno, NV) are used to provide steady laminar flow with a wall shear stress (WSS) of 10 dynes/cm^2 in a flow chamber with width of 700 μm and height of 550 μm, comprising a square glass micro-

Fig. 1 Framework to determine the force and deformation of an adherent cell under shear flow
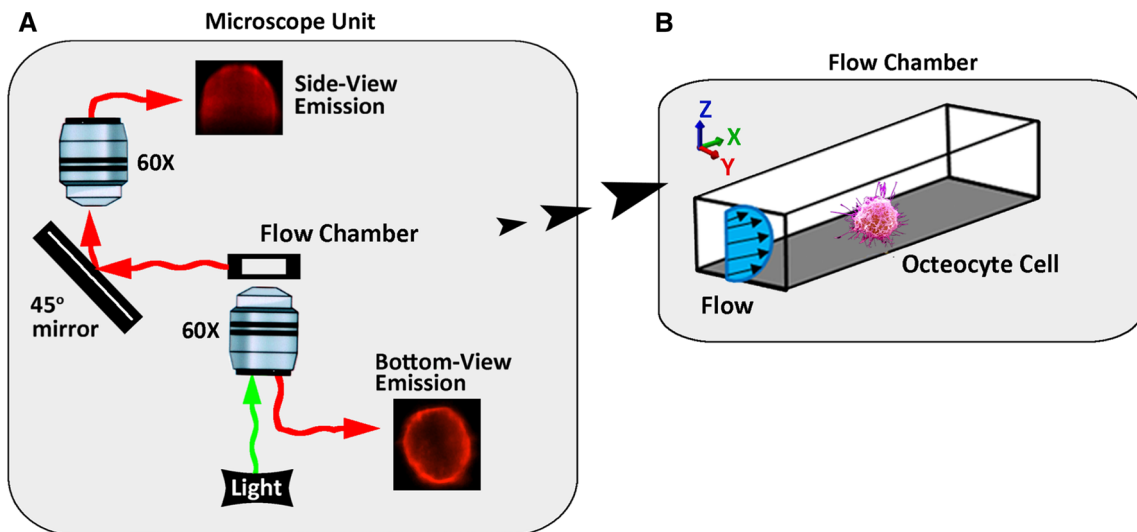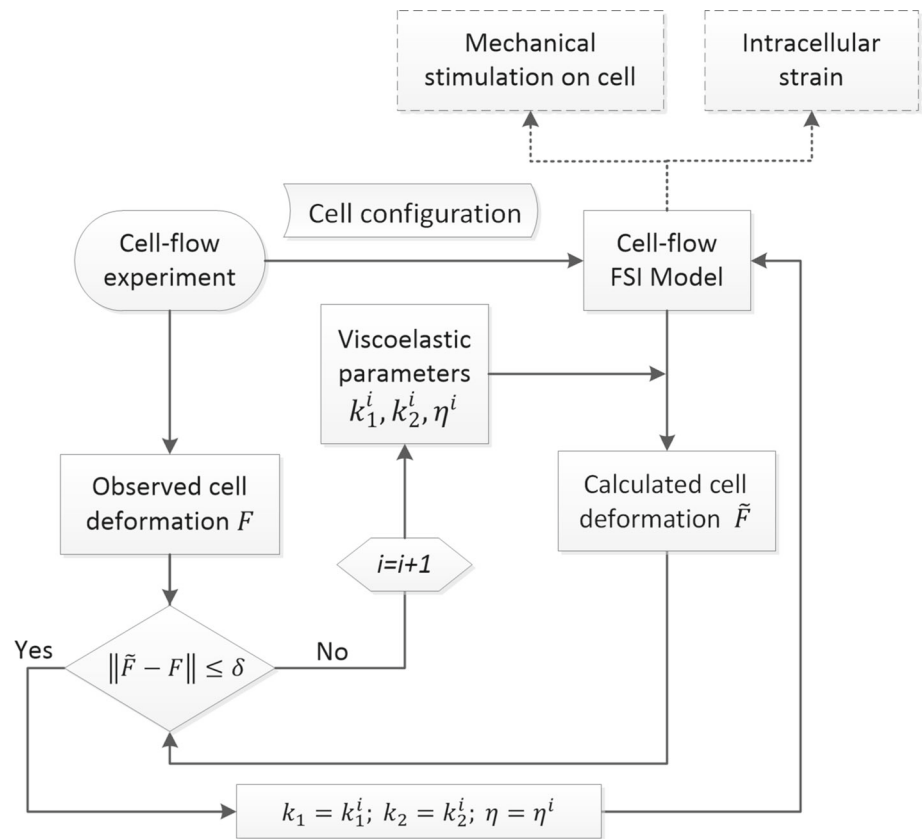
Fig. 2 Schematic of **a** the quasi-3D microscope observation system and **b** cell flow chamber experiment

tube with a glass micro-slide inside. Cells are seeded on fibronectin coated glass micro-slides for 20 min to ensure partially adherent status as in vivo and at low density to reduce the interaction between cells. Cells are stained before flow starts with Alexa Fluor 594 wheat germ agglutinin plasma membrane dye.

2.2.2 Image acquisition

The images of individual osteocytes are captured simultaneously by two microscopes in the quasi-3D microscope system introduced by Baik et al. (2010), as shown in Fig. 2. This system consists of an upright microscope and an inverted one, and a mirror is aligned at 45° in the light path of the upright

microscope to obtain side-view image, while the inverted microscope gets regular bottom-view image of the same cell. Fluorescent images with a resolution of $0.215\,\mu\text{m/pixel}$ can be captured at a frequency of 12 Hz, and then processed by digital image correlation techniques to determine the displacement of the cell contour.

2.3 3D fluid–structure interaction FE model

The assumptions below are set in the fluid–structure coupling finite element model: (1) osteocyte is a homogeneous, isotropic, and incompressible viscoelastic continuum; (2) only the passive deformation of osteocyte is analyzed without consideration of any active force; (3) the hydrodynamic properties of culture medium are equivalent to those of the water at room temperature; and (4) the environmental temperature is constant since the experiment is finished within a few minutes.
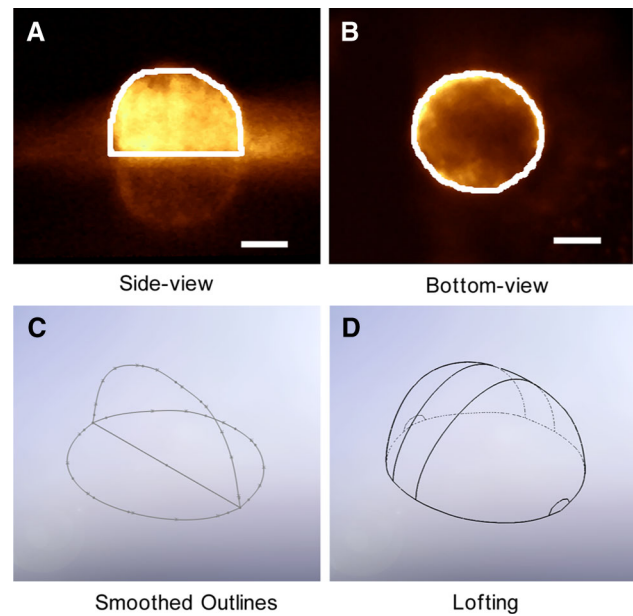
2.3.1 Cell reconstruction

Cell images in flow chamber are obtained in two perpendicular directions by the quasi-3D microscopic system. After image enhancement, the bottom and side outlines of the cell on every frame can be identified, and the 3D configurations of the cell can be reconstructed by a lofting algorithm based on cellular convexity assumptions. Microscopic observations show that the overall configuration of bone cells is quite close to ellipsoid, falling into the category of convex structures. Thus, the transition area from side to bottom outline also accords with the convexity characteristics. The reconstruction of cellular 3D configuration by bottom-view and side-view images is indicated in Fig. 3.

The white lines in Fig. 3a, b represent cell contours detected in the deformation process by digital image correlation algorithm. Subsequently, cell contours are smoothed and initialized by MATLAB (MathWorks, Natick, MA), and fitted by spline function in Slidworks (Dassault Systèmes, Concord, MA), as shown in Fig. 3c. The cell contour is finally lofted into 3D structure in Solidworks, as in Fig. 3d.

2.3.2 Structure model

Previous studies demonstrate that adherent cells exhibit viscoelastic properties (Bausch et al. 1998; Evans et al. 1984; Ward and Pinnock 1966; Yamada et al. 2000). The cell is thus assumed to be deformable with isotropic and homogeneous viscoelastic properties, which is characterized by an incompressible finite strain model (Haider and Guilak 2000; Jones et al. 1999). The relaxation shear modulus $G(t)$ of the model is represented by a one-term Prony series:

$$G(t) = G_\infty + G_1 e^{-\beta_1 t} \tag{1}$$

Fig. 3 Reconstruction of 3D cell from 2D microscopic images. **a, b** Two simultaneously obtained views of the plasma membrane of an osteocyte cell, where the *white solid lines* represent the contour of cell. **c** A typical cell profile. **d** The reconstructed 3D numerical cell. *Scale bar* is 5 μm
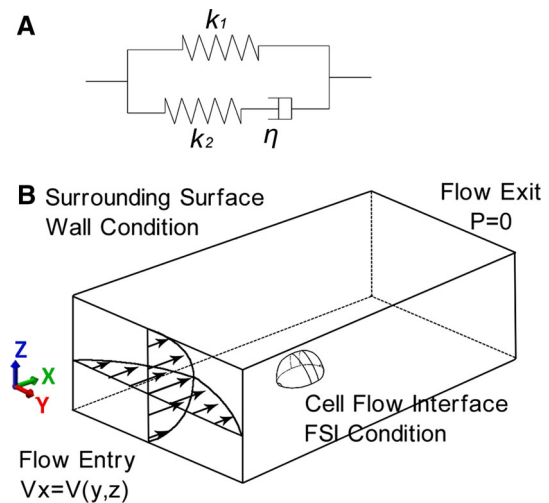
Fig. 4 Schematic of **a** standard linear solid (SLS) model and **b** the boundary condition for fluid model

The parameters of Prony series can be derived from three parameters in standard linear solid (SLS) viscoelastic model, i.e., k_1, k_2, and η, as illustrated in Fig. 4a.

2.3.3 Fluid model

The properties of the fluid medium are assumed to be equivalent to water at room temperature, i.e., an incompressible Newtonian fluid having a dynamic viscosity of $0.89 \times 10^{-3}\,\text{Pa}\cdot\text{s}$ and density of 997 kg/m^3.

Reynolds numbers (R_e) are calculated for the channel region using the formula

$$Re = \frac{\rho v L}{\eta} \tag{2}$$

where v is the mean velocity and L is the hydraulic diameter of the chamber, which is assumed to be as high as the chamber, i.e., $550\,\mu$m. The mean velocity is 57 mm/s when WSS is 10 dyn/cm^2, and the calculated R_e is around 35, indicating laminar flow and helping to determine the calculation domain.

2.3.4 Boundary conditions

The boundary conditions agree with those in the experiment. The local CFD domain is $700\,\mu$m $\times 550\,\mu$m $\times 200\,\mu$m, covering the cell deformable domain, which is adherent to the bottom of the chamber, as shown in Fig. 4b. The flow is unidirectionally in X-direction with parabolic velocity at the entrance and free of pressure at the exit.

2.3.5 Fluid–structure interaction (FSI) algorithm

In the FSI model, it is the cell membrane that acts as the fluid–solid interface, allowing the exchange of data (*i.e.*, forces and displacements) between the fluid and solid domains. The coupled simulation adopts the staggered iteration approach (Bathe 2009). Fluid equations are firstly solved to get the fluid stress tensor, which then acts on the fluid–solid interface, resulting in cellular deformation. Such deformation relays back to the fluid domain, and the fluid equations are recalculated for next iteration.

3 Results

3.1 Cell creep behavior

The adherent cell presents typical viscoelastic deformation under the fluid shear stress in the experiment. Compared with other area, the deformation on the top of the cell is the most significant, where the load-deformation path at the flow direction is shown in Fig. 5a. The steady shear flow is triggered on at the instantaneous moment t_0 and turned off at the equilibrium reaching time t_1. The flow lasts for 120 s, covering cellular instantaneous and equilibrium response. Three subgraphs (i, ii, iii) beside the curve in Fig. 5a show the specific side-view configuration of the cell at the corresponding moments. A sharp deformation can be observed at t_0, named initial jump. The deformation gradually accumulates under fluid flow and reaches equilibrium state at t_1. After the flow is off at t_1, the cellular deformation gradually recovers. It has to
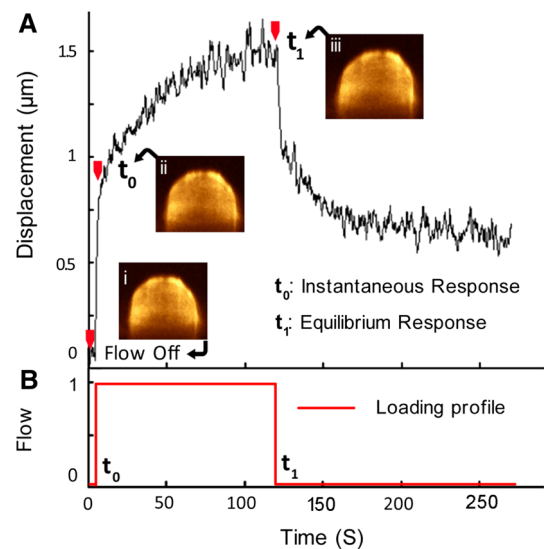

Fig. 5 **a** Viscoelastic response of cell deformation and **b** the loading profile of the flow
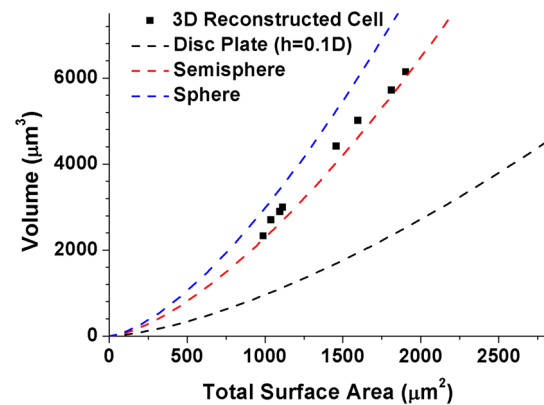

Fig. 6 Comparison of topological information among the reconstructed 3D cell, dis plate, semi-sphere, and sphere

be illustrated that throughout the entire deformation process, the cell adheres to the base steadily without any debonding.

3.2 3D cell configuration

Figure 6 shows the topological information of the reconstructed 3D cell, described by the relationship between the surface area and the volume of the cell. The black, red, and blue dash lines in Fig. 6 represent disk plate (the diameter is set as ten times of the height, i.e., $h = 0.1$D), semisphere, and sphere, respectively. The eight sample cells fall in between spherical and hemispherical, and has big disparity with disk plate, which represents completely adhesive state. It is a validation that the sample cells in experiments are in the state of partial adhesion. The volume of MLO-Y4 osteocyte cell is $4023 \pm 1487\,\mu$m^3 with the surface area of $1377 \pm 366\,\mu$m^2 (Mean $\pm$ STD, $n = 8$).
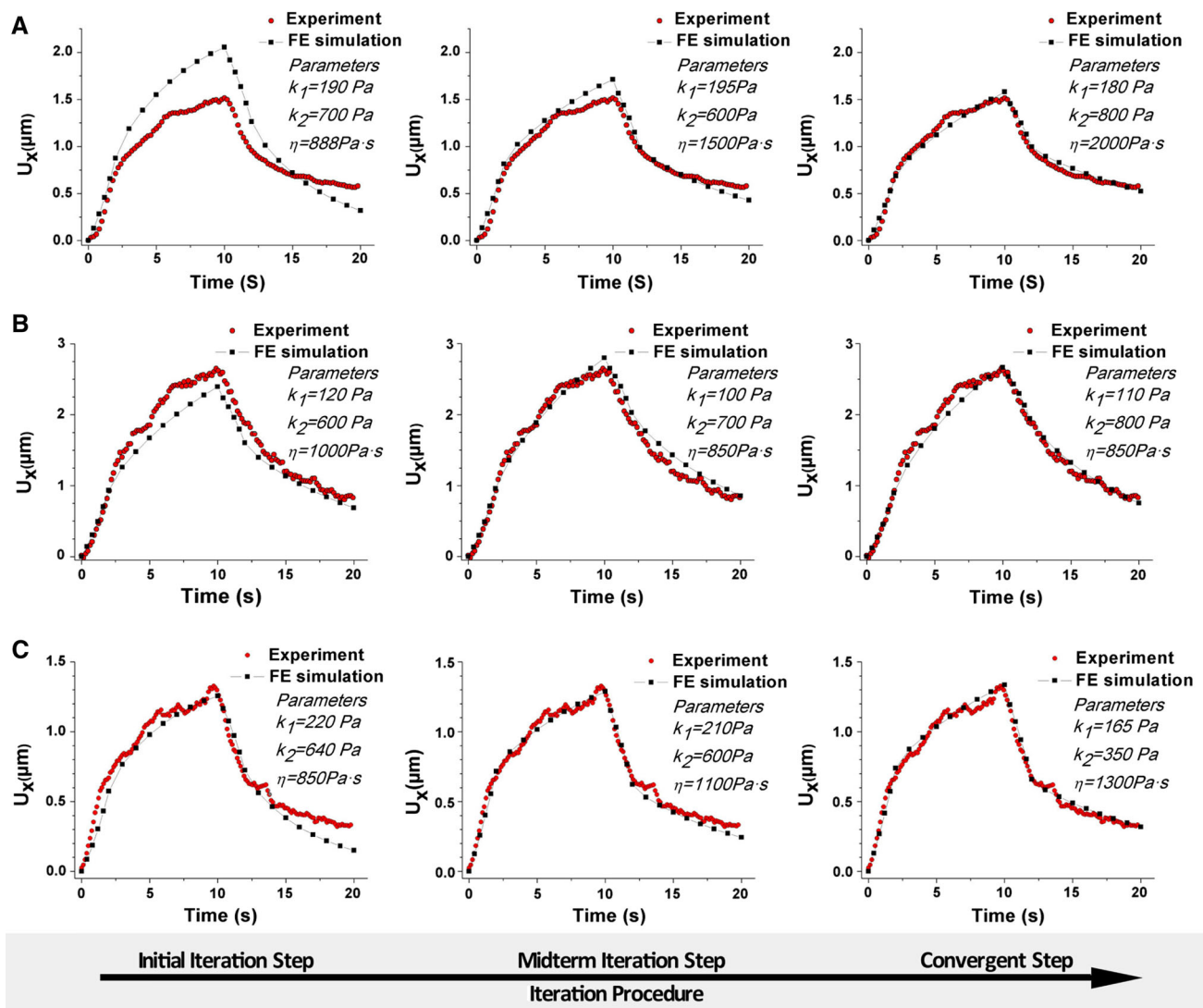
Fig. 7 Displacement–time curves of three sample cells (**a–c**) from experiment and FE simulation in the iteration process to determine cellular viscoelastic parameters

3.3 Determination of viscoelastic parameters

The creep behavior presented in Fig. 5 has demonstrated that the cell can be regarded as viscoelastic material. Three sample cells are then randomly selected to reproduce the in vitro experiments within much shorter time, 20 s, to determine the viscoelastic parameters, using the iterative method introduced in Sect. 2.1 based on the experiment in Sect. 2.2 and FE model in Sect. 2.3. The flow only lasts for 10 s for it is neither too long to induce unnecessary interference nor too short to cover up cellular viscoelasticity. The largest displacement of the three sample cells during their deformation are 1.5, 2.5 and 1.3 μm, respectively, as shown in Fig. 7. The calculated displacement curves with the initial trials have a big deviation to the experimental results, as presented in the first column in Fig. 7. Continuous iterations finally fix

a set of viscoelastic parameters, which makes the displacement curves consistent with the experimental ones, as shown in the last column in Fig. 7. The viscoelastic parameters of the osteocytic cell are: the equilibrium elasticity modulus $k_1 = 0.15 \pm 0.038$ kPa, instantaneous elasticity modulus $(k_1 + k_2) = 0.77 \pm 0.23$ kPa, $k_2 = 0.62 \pm 0.14$ kPa, creep characteristic time $\tau_\sigma = 11.30 \pm 2.34$ s, viscosity coefficient $\eta = 1.38 \pm 0.33$ kPa s.

3.4 Mechanical stimulation and response

The 3D numerical cell is constructed with the microscopic topology information and the viscoelastic parameters. The fluid–structure interaction FE model is used to analyze the interaction between cell and flow under different WSS. The WSS of the venules of human beings is about 10 dyn/cm^2

Table 1 Calculated fluid mechanical stimulation on the surface of adherent cell by FE model

V_m (mm/s)	Re	WSS (dyn/cm²)	Maximum pressure				Minimum pressure				Maximum shear stress			
			Value (dyn/cm²)	Normalized value	Position (%)		Value (dyn/cm²)	Normalized value	Position (%)		Value (dyn/cm²)	Normalized value	Position (%)	
					Xr	Zr			Xr	Zr			Xr	Zr
30	8	2.6	12.8	4.9	−72.5	79.4	−12.5	−4.8	67.8	83.6	14.8	5.7	21.2	99.4
50	14	4.5	21.2	4.7	−72.5	79.5	−21.4	−4.8	67.8	83.6	24.9	5.5	21.2	99.3
127	35	10.0	50.2	5.0	−72.5	79.5	−60.0	−6.0	67.8	83.6	62.2	6.2	21.2	99.3
200	54	17.3	81.8	4.7	−89.9	62.0	−106.0	−6.1	67.8	83.6	103.5	6.0	21.2	99.4
300	81	27.5	123.0	4.5	−89.9	62.0	−181.6	−6.6	67.8	83.6	159.7	5.8	21.2	99.3

The origin of coordinates is at the geometric center of the adherent surface of the cell, and the coordinate axis is as shown in Fig. 4b; Xr is the ratio between coordinate X and the cellular half-length, and Zr is the ratio between coordinate Z and the cellular height; normalized value is the ratio between local pressure or shear stress and the WSS; '−' means in the negative direction or negative pressure

(Koutsiaris 2015; Koutsiaris et al. 2007); thus, the cellular mechanical characteristics under different WSS conditions are studied, as shown in the third column in Table 1.

3.4.1 Mechanical stimuli on the cell flow interface

Normal pressure and shear force are two perspectives to investigate the force on the cell. The force on an adherent cell with moderate size (length in X direction $= 19.90\,\mu m$, height in Z direction $= 14.84\,\mu m$) under different flow velocity is studied, as shown in Table 1 and Fig. 8.

Table 1 presents the calculated value of the maximum and minimum pressure, and maximum shear stress, as well as the corresponding positions under different WSS. It can be seen that the pressure and shear stress on the cell are basically within 4–7 times of the WSS from Table 1. Figure 8 shows the pressure and shear stress distribution on the surface of the cell. Both the pressure and shear stress in Fig. 8 have been normalized (divided by WSS). The pressure and shear stress along the central section line of the cell in the flow direction are extracted and shown as black curves in Fig. 8b, d, respectively. The green curves represent the projection of the black curves on XZ plane, essentially the central section line of the cell. The red ones in the bottom plane represent the normalized pressure in Fig. 8b and normalized shear stress in Fig. 8d.

The extremum pressure on the cell approximately distributes in the center of the upstream side and downstream side, respectively, as shown in Fig. 8a. The position with extremum pressure almost remains the same under different flow intensity, as given in Table 1. The pressure along the central section line has a distribution similar to sinusoidal variation, as the red curve shown in Fig. 8b. The maximum shear stress appears at the top of the cell for all the WSS studied, as given in Table 1. Low shear stress (<0.45) appears at the bottom of the cell, forming a surround band, as shown in Fig. 8c. The distribution curve of the shear stress along the center section line of the cell surface is analogous to a downward parabola, as the red one in Fig. 8d.

The traction force at the mesh node in FE model is the integral value of pressure and shear stress on the cell flow interface with the magnitude of pN (10^{-12} N). Although such nodal traction force depends on the uniform size of the meshes on the interface, it can indicate the force distribution. Figure 9a–c shows the magnitude and distribution of the nodal traction force at different directions. The nodal traction force along the flow direction is dominant compared to that in other two directions.

The sum of the nodal traction force on the entire cell flow interface is the flow resultant force, the magnitude of which is determined by the interaction between flow and cell without dependence on the mesh size. The normalized flow force is defined as the ratio between the flow resultant force and the cell weight. Figure 9d presents the relationships between the normalized flow force and the WSS, indicating that normalized flow force has a positive linear correlation to WSS. With the WSS of 10 dyn/cm², equivalent to that in capillaries of human beings, the flow dragging force is almost 85 times of the cell weight in the flow direction and 3.98 times in the gravitational direction. The resultant force in flow direction is significant dominant compared to that in other two directions.

The relationship between static friction force F and normal pressure N can be expressed as $F = \mu \cdot N$ where μ is static friction coefficient. Analogy to mechanical friction, the μ between the cell and the fibronectin coated base under five WSS conditions are thus worked out to be 27.3, 25.9, 21.4, 20.1, and 18.0, respectively.

3.4.2 Intracellular strain

Figure 10 shows the distribution of intracellular strain from FE analysis, including three normal strain components in Fig. 10a–c and three shear strain components in Fig. 10d–f.
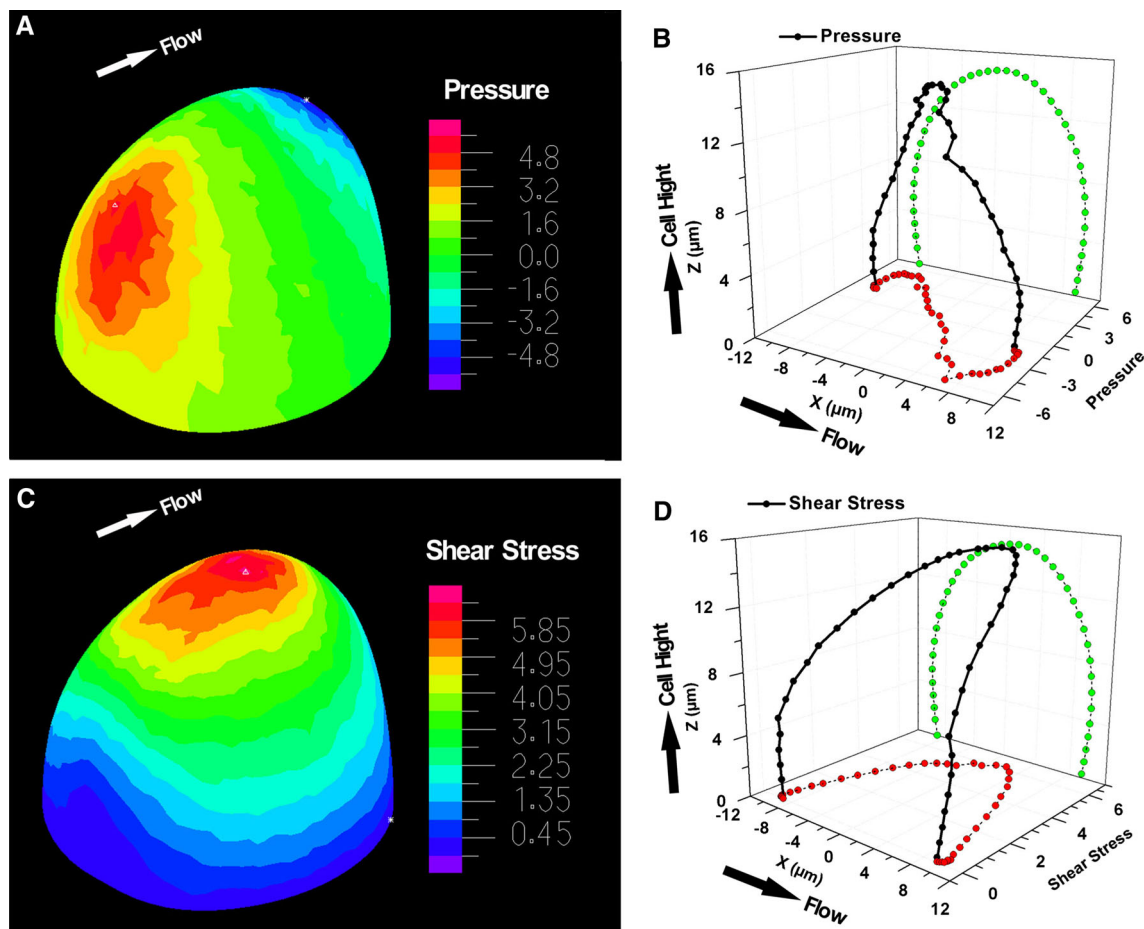
Fig. 8 Distribution of **a** normalized pressure and **c** normalized shear stress on the surface of cell from FE analysis and distribution of **b** normalized pressure and **d** normalized shear stress along the central section line of the cell

The distance between two cutting sections is 4 µm. The shear strain component E_{xz} is largest among the six strain components, about one order higher than others. The maximum E_{xz} is distributed on the upstream and downstream sides of the adherent area, where the flow shear stress is almost zero as illustrated in Fig. 8c of Sect. 3.4.1. The E_{xz} in the center of upstream and downstream surface as well as on the top of the cell is much smaller. It can be learned from Sect. 3.4.1 that the normal pressure in the center of the upstream and downstream surface is highest, and the shear stress on the top of the cell is also higher than other areas. These contradictory phenomena indicate that the stress and the strain of the adherent cell have interesting competitive relations.

4 Discussion

In this paper, a method coupling in vitro experiment and fluid–structure interaction FE model is proposed to determine the viscoelastic properties of an adherent cell under shear flow and characterize the corresponding mechanical stimuli

and the intracellular deformation. The cellular deformation in vitro experiment is recorded by a quasi-3D microscopic system. The experiment proves that the cell can be represented by viscoelastic materials. A 3D numerical cell is reconstructed on the basis of the observed cellular configuration instead of an ideal assumption of semi-sphere or sphere in the literature. Considering the fluid characteristics and boundary conditions, an FSI FE model is established. A group of viscoelastic parameters are input into this FE model to calculate the cellular deformation, which is compared to the experimental results. These parameters will be updated if the calculated deformation is greatly deviated from the observed results. Such iteration continues until the deviation is satisfying, when the viscoelastic parameters are determined. The established FSI FE model with the these parameters is then used to analyze the mechanical stimulation and response of the cell under different flow intensity.

Compared with traditional techniques measuring cellular mechanical properties, such as AFM, magnetic twist, micropipettes, and optical tweezers, the method presented in this study is nonlocal, noninvasive, and also close to the phys-
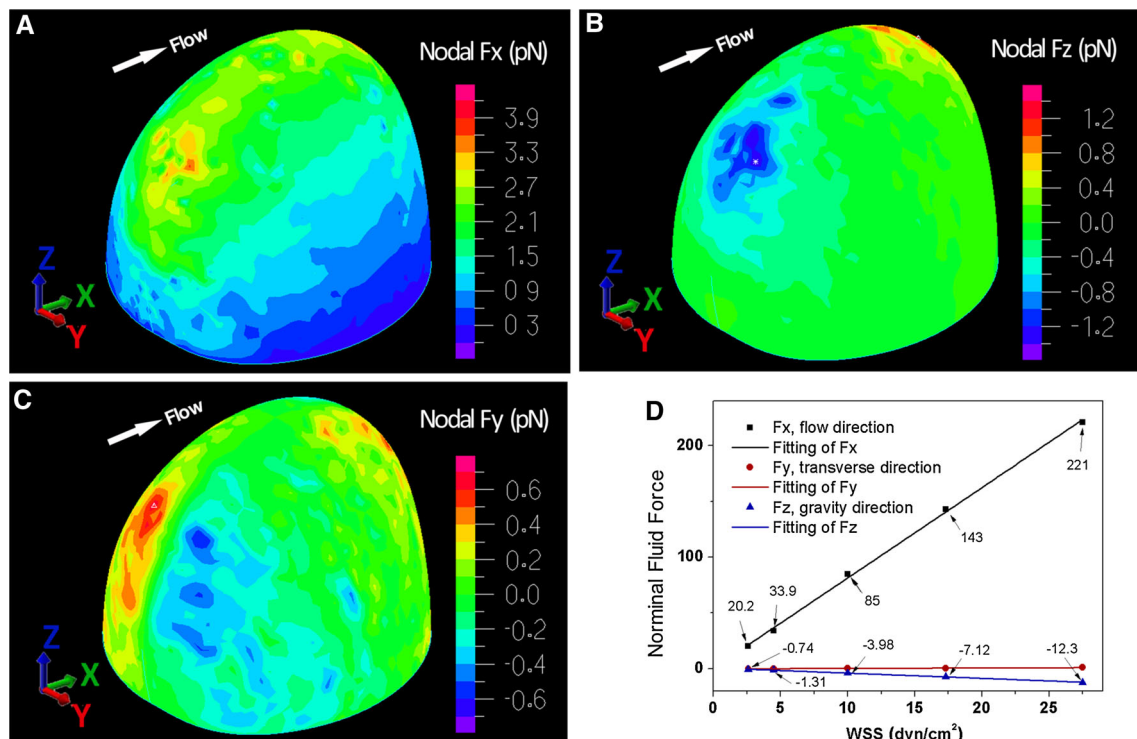
Fig. 9 Distribution of the nodal traction force on the interface between cell and flow from FE analysis in **a** flow direction, **b** gravity direction, and **c** transverse direction; **d** the relationship between the nominal flow force and WSS, the sample cell weight is 29 pN

iological conditions in vivo; cellular responses under shear flow are the mechanical behavior of the entire cell instead of a particular local part; no external objects such as probes, beads, or pipettes are used to apply loads onto the sample cells; last but not least, the force is applied naturally to the cellular surface by fluid flow, the process of which is similar to the physiological interaction between osteocytes and their microenvironment.

Researches on the mechanical properties of osteocytes are relatively rare. Previous studies reported the elastic constant of MLO-Y4 round but partially adherent osteocytes is below 1 kPa by AFM (Bacabac et al. 2008). In our previous work, the modulus of the same kind of cell is 0.49 ± 0.11 kPa based on an computational optimization method (Qiu et al. 2014), the objective function of which is conducted by cell deformation configuration. In this study, the instantaneous modulus of partially adherent MLO-Y4 osteocytes is 0.77 ± 0.23 kPa, close to our reported data but with much lower computational cost. In addition to the instantaneous modulus, we also studied the elastic modulus in equilibrium state ($K_1 = 0.15 \pm 0.038$ kPa) and the creep characteristic time ($\tau_\sigma = 11.30 \pm 2.34$ s), which reflects cellular viscosity coefficient ($\eta = 1.38 \pm 0.33$ kPa s).

Through this study, osteocytes (<1 kPa) are found to be softer than osteoblasts (>1 kPa) (Darling et al. 2008) with smaller elastic modulus. Previous studies have demonstrated that osteocytes are evolved from osteoblasts by burying itself in lacunae within the bone matrix (Guilak and Mow 2000). It implies that some changes might occur to the cytoskeleton of the osteoblasts after being embedded in bone mineral to improve its sensitivity to extracellular stimulations. Furthermore, another interesting thing is that the mechanical properties of osteocytes and chondrocytes (<1 kPa) (Trickey et al. 2000) are ranged in the same level although they belong to different organizations. Osteocytes and chondrocytes have similar external mechanical environment, i.e., they are embedded in bone lacuna and cartilage lacuna, respectively. Thus, the cellular mechanical properties might have strong correspondence with the external microenvironment of cells.

According to the calculated results from FSI FE model, the flow dragging force on the cell is about 85 times of the cell weight under the WSS of 10 dyn/cm^2, and the corresponding static friction coefficient is over 20. It is one order higher than the friction coefficient between pure surfaces of inorganic materials under high-vacuum state. The biological binding, focal adhesion, between the cell and the substrate must be the reason for such high friction coefficients. The approach proposed in this study also provides an accurate method to quantify such bonding strength using experiments and FE models.
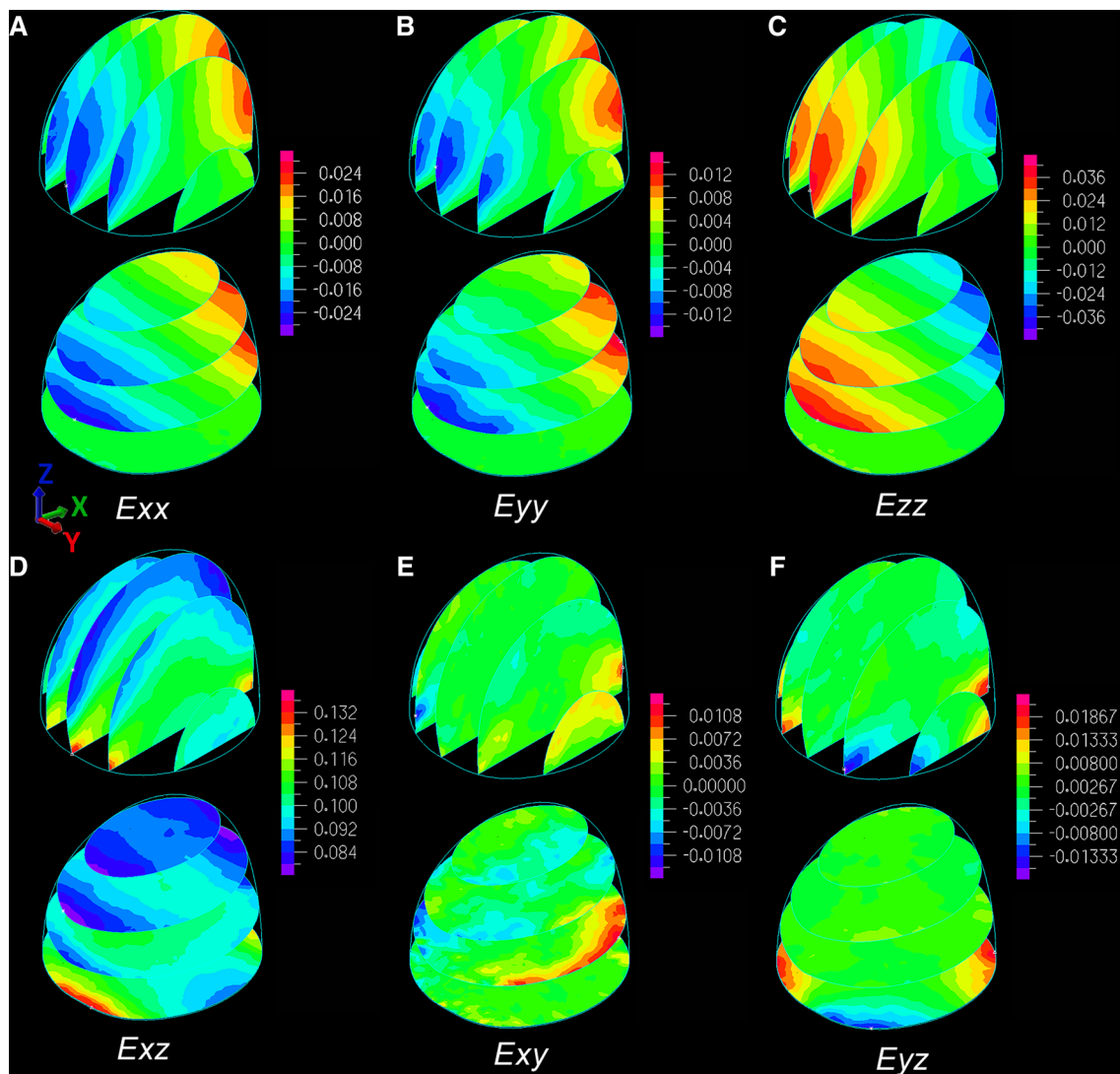
Fig. 10 Distribution of intracellular strain

Identification of whether the cellular response is a strain-activated or stress-activated mechanism under fluid flow appears difficult since it is hard to acquire stress and strain simultaneously. De et al. (2008) discussed whether the cellular orientation responds to strain or stress of the matrix, and reported that the cellular orientation is a strong function of the Poisson's ratio v of the matrix when cell activity is governed by the matrix strain, while if cell activity is governed by the matrix stress, the orientation depends only weakly on v. McGarry et al. (2005) tested the hypothesis that bone cells respond differently to 0.6 Pa fluid shear stress and 1000 $\mu\varepsilon$ substrate strain stimulation because of the qualitative and quantitative differences of the cellular deformation. Our study highlights the distribution properties of the stress and strain of MLO-Y4 osteocytes under fluid flow in vitro. A significant phenomenon is that the distribution of stress on the cell is inconsistent with that of the intracellular strain.

The highest shear stress is found at the top of the cell as shown in Fig. 8c, while the highest intracellular strain distributes at the upstream and downstream interface between the cell and the substrate as in Fig. 10d. Based on the assumption that cell could sense the extracellular mechanical signals more easily from the membrane domain where the signals are the strongest, there might exist two mechanical signaling channels. One is sensitive to stress from apical region to the nucleus area, and the other is sensitive to strain from the bottom of the cell to the nucleus area. This provides a unique perspective to understand the mechanisms of mechanotransduction particularly for the partially adherent cells under fluid flow.

The current FSI FE model combined with experiments provides a quantitative approach to determine cell mechanical properties and illustrate general features of the stress and strain distributions of adherent cells under fluid flow. Poten-

tial limitations of this study are mainly concerned with the numerical model, in particular the representation of a single cell as homogeneous and isotropic continuum. Future studies could enrich the model with certain crucial details, such as cell nucleus, cytoplasm, cytomembrane, and primary cilia (Jacobs et al. 2010). Furthermore, a certain degree of viscoplastic behavior has also been observed in our experiments rather than completely viscoelastic property, which can also be taken into account in the future. It is believed that this work not only quantifies the cellular mechanical characteristics with higher accuracy but also helps to elucidate the mechanisms of mechanotransduction for various adherent cells.

Compliance with ethical standards

Conflict of interest None.

References

Anderson EJ, Falls TD, Sorkin AM, Tate MLK (2006) The imperative for controlled mechanical stresses in unraveling cellular mechanisms of mechanotransduction. Biomed Eng Online 5:27. doi:10.1186/1475-925x-5-27

Baaijens FPT, Trickey WR, Laursen TA, Guilak F (2005) Large deformation finite element analysis of micropipette aspiration to determine the mechanical properties of the chondrocyte. Ann Biomed Eng 33:494–501. doi:10.1007/s10439-005-2506-3

Bacabac RG, Mizuno D, Schmidt CF, MacKintosh FC, Van Loon JJ, Klein-Nulend J, Smit TH (2008) Round versus flat: bone cell morphology, elasticity, and mechanosensing. J Biomech 41:1590–1598

Baik AD, Lu XL, Qiu J, Huo B, Hillman E, Dong C, Guo XE (2010) Quasi-3D cytoskeletal dynamics of osteocytes under fluid flow. Biophys J 99:2812–2820

Bathe KJ (ed) (2009) Volume III: ADINA CFD & FSI vol III. Theory and modeling guide. ADINA R&D, Inc

Bausch AR, Ziemann F, Boulbitch AA, Jacobson K, Sackmann E (1998) Local measurements of viscoelastic parameters of adherent cell surfaces by magnetic bead microrheometry. Biophys J 75:2038–2049

Bonewald LF, Kato Y (2002) U.S. Patent No. 6,358,737. U.S. Patent and Trademark Office, Washington, DC

Charras G, Horton M (2002) Determination of cellular strains by combined atomic force microscopy and finite element modeling. Biophys J 83:858–879

Cowin S, Telega J (2003) Bone mechanics handbook. Appl Mech Rev B56:B61–B63

Darling E, Zauscher S, Guilak F (2006) Viscoelastic properties of zonal articular chondrocytes measured by atomic force microscopy. Osteoarthr Cartil 14:571–579

Darling EM, Topel M, Zauscher S, Vail TP, Guilak F (2008) Viscoelastic properties of human mesenchymally-derived stem cells and primary osteoblasts, chondrocytes, and adipocytes. J Biomech 41:454–464. doi:10.1016/j.jbiomech.2007.06.019

De R, Zemel A, Safran SA (2008) Do cells sense stress or strain? Measurement of cellular orientation can provide a clue. Biophys J 94:L29–L31. doi:10.1529/biophysj.107.126060

Evans E, Mohandas N, Leung A (1984) Static and dynamic rigidities of normal and sickle erythrocytes. Major influence of cell hemoglobin concentration. J Clin Investig 73:477

Evans E, Yeung A (1989) Apparent viscosity and cortical tension of blood granulocytes determined by micropipet aspiration. Biophys J 56:151–160

Guck J et al (2005) Optical deformability as an inherent cell marker for testing malignant transformation and metastatic competence. Biophys J 88:3689–3698

Guilak F (1995) Compression-induced changes in the shape and volume of the chondrocyte nucleus. J Biomech 28:1529–1541

Guilak F, Mow VC (2000) The mechanical environment of the chondrocyte: a biphasic finite element model of cell–matrix interactions in articular cartilage. J Biomech 33:1663–1673

Haider MA, Guilak F (2000) An axisymmetric boundary integral model for incompressible linear viscoelasticity: application to the micropipette aspiration contact problem. J Biomech Eng 122:236–244

Hazel AL, Pedley TJ (2000) Vascular endothelial cells minimize the total force on their nuclei. Biophys J 78:47–54

Hochmuth RM (2000) Micropipette aspiration of living cells. J Biomech 33:15–22

Jacobs CR, Temiyasathit S, Castillo AB (2010) Osteocyte mechanobiology and pericellular mechanics. Annu Rev Biomed Eng 12:369–400

Jones WR, Ping Ting-Beall H, Lee GM, Kelley SS, Hochmuth RM, Guilak F (1999) Alterations in the Young's modulus and volumetric properties of chondrocytes isolated from normal and osteoarthritic human cartilage. J Biomech 32:119–127

Koay EJ, Shieh AC, Athanasiou KA (2003) Creep indentation of single cells. J Biomech Eng 125:334–341

Koutsiaris A (2015) Wall shear stress in the human eye microcirculation in vivo, segmental heterogeneity and performance of in vitro cerebrovascular models. Clin Hemorheol Microcirc 63:15–33

Koutsiaris AG, Tachmitzi SV, Batis N, Kotoula MG, Karabatsas CH, Tsironi E, Chatzoulis DZ (2007) Volume flow and wall shear stress quantification in the human conjunctival capillaries and postcapillary venules in vivo. Biorheology 44:375–386

Lulevich V, Zink T, Chen H-Y, Liu F-T, Liu G-y (2006) Cell mechanics using atomic force microscopy-based single-cell compression. Langmuir 22:8151–8155

Mahaffy R, Park S, Gerde E, Käs J, Shih C (2004) Quantitative analysis of the viscoelastic properties of thin regions of fibroblasts using atomic force microscopy. Biophys J 86:1777–1793

McGarry JG, Klein-Nulend J, Mullender MG, Prendergast PJ (2005) A comparison of strain and fluid shear stress in stimulating bone cell responses-a computational and experimental study. FASEB J 19:482–484

Qiu J, Baik AD, Lu XL, Hillman E, Zhuang Z, Dong C, Guo XE (2014) A noninvasive approach to determine viscoelastic properties of an individual adherent cell under fluid flow. J Biomech 47:1537–1541

Qiu J, Baik AD, Lu XL, Hillman EMC, Zhuang Z, Dong C, Guo XE (2012) Theoretical analysis of novel quasi-3D microscopy of cell deformation. Cell Mol Bioeng 5:165

Sato M, Theret D, Wheeler L, Ohshima N, Nerem R (1990) Application of the micropipette technique to the measurement of cultured porcine aortic endothelial cell viscoelastic properties. J Biomech Eng 112:263

Shin D, Athanasiou K (1999) Cytoindentation for obtaining cell bio-mechanical properties. J Orthop Res 17:880–890

Theret DP, Levesque M, Sato M, Nerem R, Wheeler L (1988) The application of a homogeneous half-space model in the analysis of endothelial cell micropipette measurements. J Biomech Eng 110:190–199

Trickey WR, Lee GM, Guilak F (2000) Viscoelastic properties of chondrocytes from normal and osteoarthritic human cartilage. J Orthop Res 18:891–898. doi:10.1002/jor.1100180607

Vargas-Pinto R, Lai JL, Gong HY, Ethier CR, Johnson M (2015) Finite element analysis of the pressure-induced deformation of Schlemm's canal endothelial cells. Biomech Model Mechanobiol 14:851–863. doi:10.1007/s10237-014-0640-2

Ward I, Pinnock P (1966) The mechanical properties of solid polymers. Br J Appl Phys 17:3

Weinbaum S, Cowin S, Zeng Y (1994) A model for the excitation of osteocytes by mechanical loading-induced bone fluid shear stresses. J Biomech 27:339–360

Wu JZ, Herzog W (2006) Analysis of the mechanical behavior of chondrocytes in unconfined compression tests for cyclic loading. J Biomech 39:603

Yamada S, Wirtz D, Kuo S (2000) Mechanics of living cells measured by laser tracking microrheology. Biophys J 78:1736–1747

You L, Temiyasathit S, Lee P, Kim CH, Tummala P, Yao W, Kingery W, Malone AM, Kwon RY, Jacobs CR (2008) Osteocytes as mechanosensors in the inhibition of bone resorption due to mechanical loading. Bone 42:172–179

Zhao R, Wyss K, Simmons CA (2009) Comparison of analytical and inverse finite element approaches to estimate cell viscoelastic properties by micropipette aspiration. J Biomech 42:2768–2773